PERGAMON

International Journal of Solids and Structures 38 (2001) 9133–9148

INTERNATIONAL JOURNAL OF SOLIDS and STRUCTURES

www.elsevier.com/locate/ijsolstr

Solutions for contact in pinned connections

K. Iyer *

Department of Mechanical Engineering, University of Michigan, 2250 G.G. Brown Building, 2350 Hayward Street, Ann Arbor, MI 48109-2125, USA

Received 9 November 2000

Abstract

The pinned connection is a principal joining and load-bearing element in countless structures. A comprehensive analytical solution for the mechanics of a pinned connection would greatly facilitate mechanics and dynamics analyses seeking to address larger issues such as fatigue life and earthquake resistance of entire structures. However, even the most advanced closed-form solutions describing contact conditions in pinned connections involve mathematical approximations for some or all of the following aspects of the problem: plate dimensions, contact area, pin–plate friction and material–property mismatch. The actual problem involving a finite plate, frictional contact and arbitrary material pairs still remains intractable in a rigorous manner through elasticity theory. This study uses the finite element method to obtain solutions when some or all of the above simplifying assumptions are removed, and thereby also evaluates the general applicability of the most advanced closed-form solutions. A surprising finding is that the pin–plate contact pressure and plate tangential stress distributions are practically independent of the material pair as long as both the pin and plate are metallic and the friction coefficient is small. It is also found that the stress concentration factor in the plate is significantly higher when finite dimensions are considered. Among the factors considered, the pin–plate friction coefficient has the greatest effect on the contact pressure and tangential stress distributions.

Keywords: Mechanical fastening; Finite plate; Frictional contact; Dissimilar materials

1. Introduction

Pinned connections represent three-dimensional double shear joints or two-dimensional analogues of single shear joints that constitute an enormous variety of engineered structures including the skeletal frameworks and outer skins of spacecraft, aircraft, automobiles, ships, pressure vessels, buildings, etc. The stresses and slips in the vicinity of contact regions determine the static strength, cyclic plasticity, frictional damping and vibration levels associated with these structures and therefore directly affect crucial structural

* Tel.: +1-734-615-2485; fax: +1-734-615-4891.
E-mail address: kiyer@umich.edu (K. Iyer).

0020-7683/01/$ - see front matter
PII: S0020-7683(01)00054-3

performance metrics as diverse as fatigue life, positioning and guidance accuracies and earthquake resistance (Crawley et al., 1983; Shin et al., 1991; Folkman et al., 1995; Schijve, 1996; Lin et al., 1997; Gaul et al., 1998). The primary metric of a pinned connection is related to its application. In aircraft and rotorcraft structures, high fatigue and fretting resistance are desired to ensure safety and maximize component life. However, frictional damping in each connection also affects performance characteristics such as noise and vibration levels. In nominally static structures such as bridges, high static strength is of primary consideration although fatigue susceptibility cannot be neglected at the design stage – bridge failures have been known to occur due to fatigue when the frequency of a cyclic load matches the natural frequency of the structure. The stress concentration in the plate determines the static and fatigue strength of a pinned connection. The contact pressure and friction coefficient determine frictional damping and susceptibility to fretting damage.

The pinned connection is rarely of interest in isolation since most real structures consist of tens to thousands of pinned connections, and it is the behavior of an entire structure that is of ultimate consequence. Yet faithful modeling of each connection in a structure is computationally prohibitive, and in this regard, closed form or analytical expressions that capture the essential aspects of each pinned connection are extremely valuable since they are amenable to inexpensive numerical representation. Unfortunately, all presently available closed-form solutions for an elastic pinned connection suffer from one or more serious limitations that result from assumptions made to simplify the mathematical procedure. In particular, they have been obtained by assuming one or more of the following: (i) frictionless contact, (ii) elastic similarity between the pin and plate, and (iii) infinite plate dimensions. It is clear that each of these factors can affect the strength, fatigue life, etc., of a joint or structure significantly and therefore cannot be neglected in design.

The purpose of this study is to evaluate contact conditions in more realistic pinned connections. This is done from the perspective of future extensions of existing closed-form solutions to the large variety of joint and structural design issues. The finite element method is used to evaluate the effects of parameters that are presently beyond the scope of a non-numerical treatment.

2. Background

Ever since the solution for the stress concentration at a hole in an infinite plate (Timoshenko and Goodier, 1961), several analytical and experimental studies have approached the problem that arises next as a logical progression, i.e. that of a pinned connection. The two-dimensional elastic contact of a circular pin contained within a circular hole in an infinite plate involves conforming boundaries and is a problem where neither body can be treated as a semi-infinite half space. These two characteristics place the problem outside the scope of Hertzian contact theory (Johnson, 1985).

In the simplest analytical formulation, the elastic pinned connection problem considers an infinite plate, identical pin and plate materials and frictionless contact; the pin is usually forced against the plate by a concentrated load applied at its center. The complexity of the analytical problem grows dramatically when one begins to consider interfacial friction, arbitrary pin materials and a finite plate. For a substantial review of the open literature (experimental and analytical studies) on the pinned connection problem, the reader can refer to a recent paper by Ho and Chau (1997). What is striking is that the scope of available solutions has tended to remain highly restricted – approximate solutions exist for frictional contact or arbitrary pin material or a finite strip, but the most advanced exact solution is valid only for an infinite sheet and frictionless contact and elastic material similarity. Further, the accuracy of the approximate solutions is still open to question because of limited means of validation.

Among the entire set of solutions available, two new closed-form solutions have appeared recently that represent major advances. One, by Ciavarella and Decuzzi (2000), extends Persson's (Johnson, 1985) solution to the case of elastically similar pin and plate materials; an infinite plate and frictionless contact are remaining limitations. The approach used here is classical for contact problems and involves the inversion of a singular integral equation for the contact pressure, from which the contact angle and tangential stress can be obtained. The second, by Ho and Chau (1997), does not solve the actual contact problem but superposes solutions for two bonded-inclusion problems employing novel force potentials to provide an approximate closed-form solution for arbitrary pin (inclusion) materials and frictional contact. This approach also assumes semi-circular contact and contains a non-physical relationship between friction coefficient and material constants. The approximations notwithstanding, the solution by Ho and Chau is the only one in closed form yet to account for frictional contact and an arbitrary pin material. It is relevant to note that available closed-form solutions with a finite sheet employ an approach similar to Ho and Chau but neglect friction and dissimilar materials (Ho and Chau, 1997).

While obtaining closed-form solutions when a finite plate, arbitrary pin material or frictional contact is involved pose significant theoretical and mathematical challenges that are unlikely to be overcome in the short term, the solution for the entire pinned connection problem can already be obtained using the finite element method. The main consideration here is the accuracy of the numerical solution owing to the highly non-linear nature of contact stresses. This study uses the finite element method to study the pinned connection. After validating the finite element model by comparison with the above-cited solutions, within the scope of their applicability, the effects of frictional contact, elastic material dissimilarity, finite sheet dimensions and biaxial loading on the contact pressure and tangential stress distributions are evaluated.

3. Finite element analysis

The two-dimensional pinned connection finite element model used in this study is shown in Fig. 1. It was developed for use with the ABAQUS code. Two sets of finite element analyses were performed – one involving an infinite plate and another involving a plate with finite dimensions. Both the pin and plate were considered to be in plane strain. This was an arbitrary choice since obtaining a full plane stress or combined (pin in plane strain) solution does not represent any additional difficulty. The in-plane dimensions used for the finite plate, hole radius and pin radius are indicated in Fig. 1. Only the case of equal pin and hole radii was considered since this was sufficient for the present purposes. The pin/hole radius, R, and finite sheet dimensions shown in Fig. 1 were derived from typical airframe riveted connections. Within each of the two sets of analyses, three values of friction coefficient ($\mu = 0$, 0.2 and 1) and four typical combinations of pin–plate materials (aluminum–aluminum, steel–aluminum, titanium–aluminum and aluminum–epoxy) were considered. A Coulomb friction model was assumed. For calculations involving a finite plate, the pin was held fixed at its center while a tensile stress of 60 MPa was applied at the far edge of the plate along its longitudinal (2-)direction. This stress corresponds to a load per unit thickness of the plate, Q, of 1836 kN. For an infinite plate, a statically equivalent concentrated load, $Q = 1836$ kN, was applied to the center of the pin while the far edge of the plate was held fixed in the 2-direction. Finally, a few calculations were performed with the finite plate with its sides held fixed in the lateral (1-axis) direction in addition to the longitudinal, uniaxial stress. The added boundary condition represents the constraints that would be present when several pins are arranged in a row. Since the displacement constraints on the sides of the plate induce a stress in the plate in the 1-direction

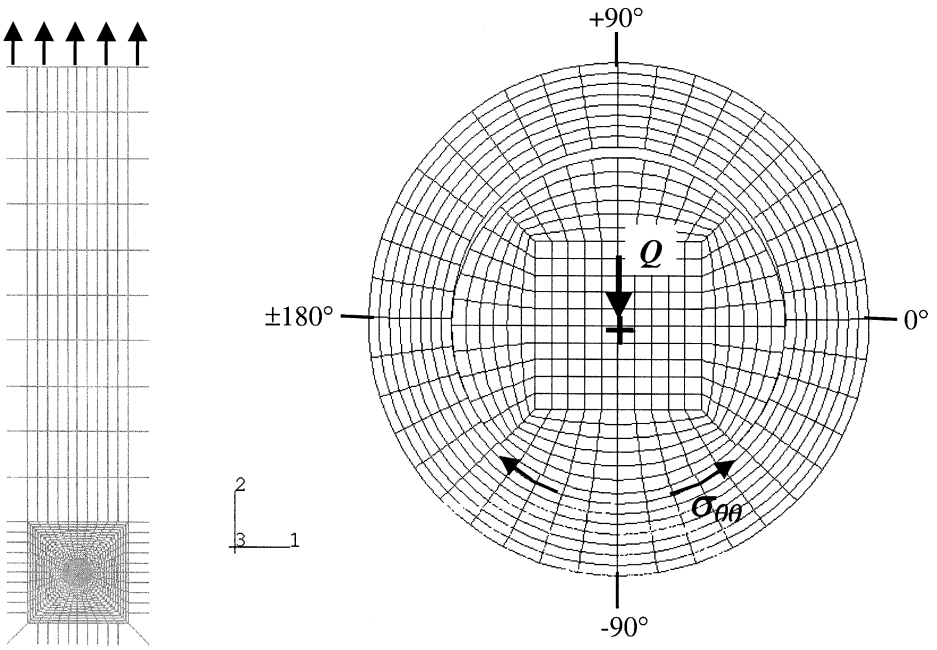

Fig. 1. Finite element model of the pinned connection. The plate consists of a region with finite dimensions bounded by infinite finite elements. When the plate is finite (minus infinite elements), it is 30.6 mm wide and 168.3 mm long. The center of the hole (and pin) is 15.3 mm from the lower edge and each of the sides of the plate in this case. The radius of the hole is $R = 3.06$ mm. A section of the deformed mesh near the contact region is shown on the right. The angular location convention and tangential stress around the hole, $\sigma_{\theta\theta}$, are also shown.

Table 1
The combinations of elastic material properties considered in the analyses

Case #	E_1 (GPa)	E_2 (GPa)	ν_1	ν_2	α	β
1	70	70	0.31	0.31	0	0
2	207	70	0.25	0.43	−0.44	0
3	207	70	0.33	0.31	−0.5	−0.29
4	117	70	0.31	0.31	−0.25	−0.14
5	70	3	0.31	0.36	−0.91	−0.40

Subscripts 1 and 2 refer to the pin and plate respectively.

also, the plate was in a state of biaxial stress in these cases. The resulting biaxiality ratio, $(\sigma_{11}/\sigma_{22})$, was 1/3.

Table 1 shows the material combinations and Dundurs' constants, α and β (Barber, 1992), used for this analysis. The two constants are defined as

$$\alpha = \frac{E_2(1-\nu_1^2) - E_1(1-\nu_2^2)}{E_2(1-\nu_1^2) + E_1(1-\nu_2^2)} \tag{1}$$

and

$$\beta = \frac{E_2(1-2\nu_1)(1+\nu_1) - E_1(1-2\nu_2)(1+\nu_2)}{E_2(1-\nu_1^2) + E_1(1-\nu_2^2)} \tag{2}$$

The two constants reflect the similarity in the elastic modulus, E, and Poisson's ratio, ν, for a pair of materials. In the present study, where subscripts 1 and 2 refer to the pin and plate, respectively, α and β will always be negative when the pin is stiffer than the plate. The absolute values of α and β increase with the degree of material dissimilarity.

4. Model validation

The accuracy of the finite element model used for the study was determined by comparing computed results for the pin–plate contact pressure with the closed-form results by Ciavarella and Decuzzi (2000) and Ho and Chau (1997).

The closed-form solution by Ciavarella and Decuzzi (2000) is valid only when $\beta = 0$, friction coefficient, μ, is 0, and the plate is infinite. If $\beta = 0$, Eq. (2) reduces to

$$\frac{E_2}{E_1} = \frac{(1-2\nu_2)(1+\nu_2)}{(1-2\nu_1)(1+\nu_1)} \tag{3}$$

Table 1 shows two sets of conditions that were considered for validation purposes. Case 1 is the trivial case where the pin and plate have identical material properties and Eqs. (1) and (2) reduce to $\alpha = \beta = 0$. For case 2, values of E_1 and E_2 were chosen to represent steel and aluminum alloys, respectively, and a value of $\nu_1 = 0.25$ was assumed. The resulting quadratic equation (3), was solved to obtain the values of ν_2 and α listed for case 2.

Table 2 and Fig. 2 demonstrate the good agreement between the closed-form solution by Ciavarella and Decuzzi and the present finite element solution. In Table 2, p_0 and θ_0 refer to the peak contact pressure and contact semi-angle, respectively. The contact width is related to the contact semi-angle and is equal to ($\frac{2\pi\theta_0}{180}$ 3.06) mm. The distance between adjacent nodes of the finite element model along the contact interface is approximately 240 μm ($= \frac{\pi(4.5^\circ)}{180^\circ}$ 3.06 mm). The resolution of the computed results is limited by this value. A minor difference in the shape of the contact pressure distribution near the contact boundary is noted; the computed solution falls to zero at the edge of the contact less abruptly than the analytical solution.

Fig. 2(a) also compares the computed contact pressure distribution with the approximate solution by Ho and Chau (1997). Ho and Chau assume semi-circular contact a priori, i.e. $\theta_0 = 90^\circ$, and a sinusoid-based representation for the contact pressure. It can be seen that this approximate closed-form solution differs from the finite element solution and the one by Ciavarella and Decuzzi significantly. The present finite element solution and the one by Ciavarella and Decuzzi thus validate each other.

Table 2
Comparison of computed and analytical values for the normalized peak contact pressure, $p_0 \cdot R/Q$, and angular location of the contact boundary, θ_0

Case #	$p_0 \cdot R/Q$		θ_0 (°)	
	Computed	Analytical	Computed	Analytical
1	0.601	0.599	85.5	84.83
2	0.618	0.616	81.0	78.56

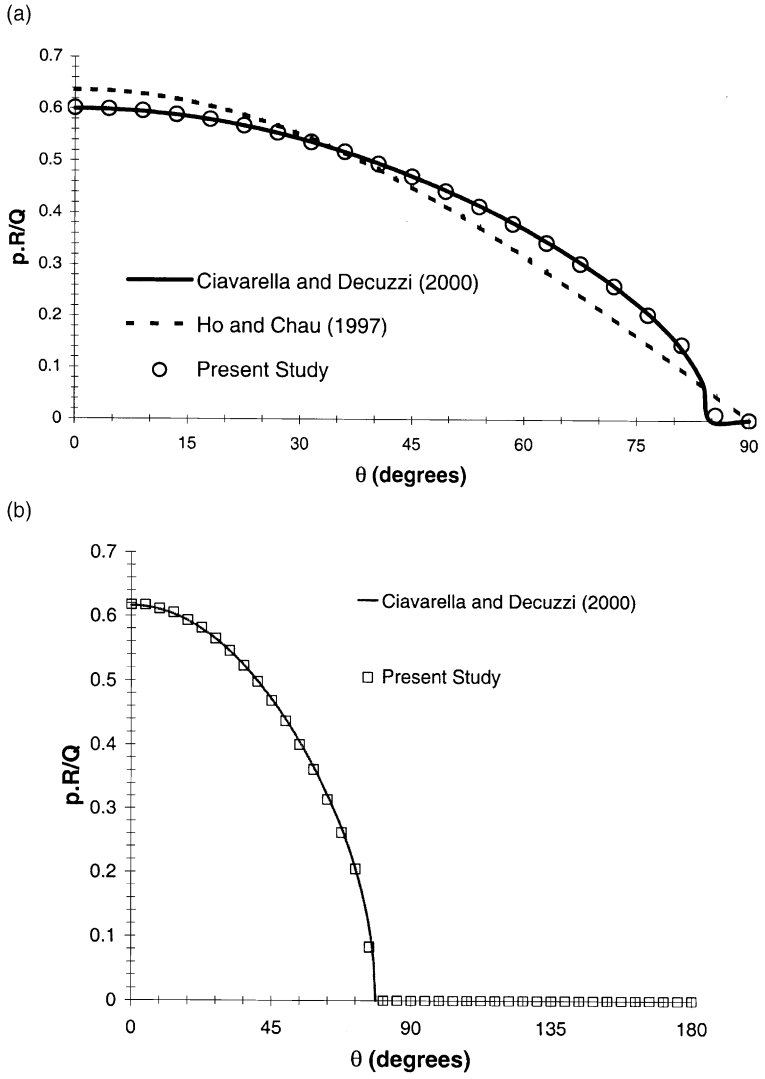

Fig. 2. Comparison of the finite element and analytical solutions for the pin–plate contact pressure. (a) $\alpha = \beta = 0$ (case 1), (b) $\alpha \neq \beta = 0$ (case 2).

5. Results

The effects of the friction coefficient, μ, pin–plate material combinations, finite plate dimensions and biaxial loading on the normalized contact pressure, $p \cdot R/Q$, contact angle, θ_0, and the normalized tangential stress around the hole, $\sigma_{\theta\theta} \cdot R/Q$, are summarized in Figs. 3 and 4.

5.1. Contact pressure distribution

Effects of friction: Fig. 3(a) shows the effect of the friction coefficient, μ, on the normalized contact pressure, $p \cdot R/Q$, for an all-aluminum alloy connection with an infinite plate. It can be seen that the peak

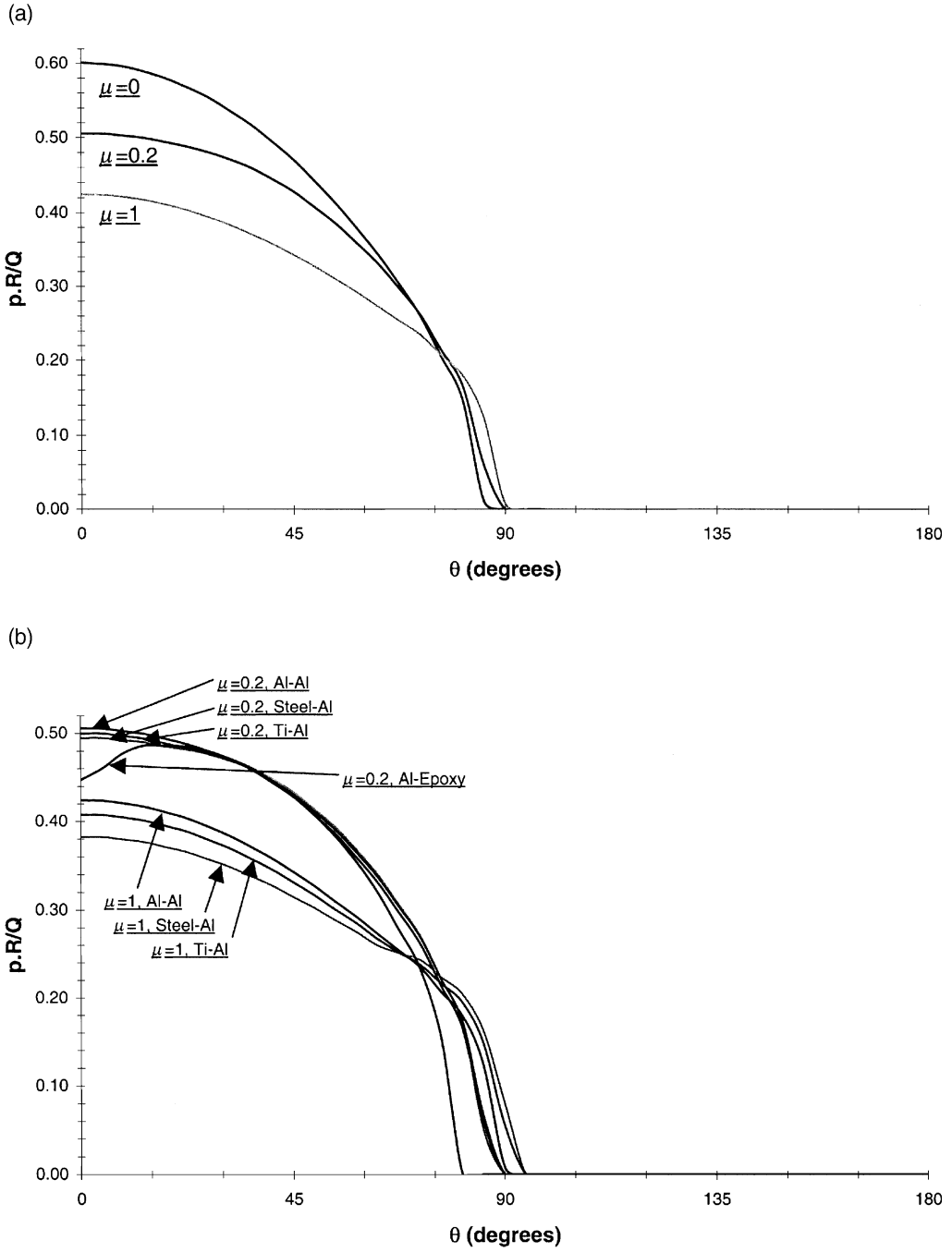

Fig. 3. Normalized pin–plate contact pressure, $p \cdot R/Q$, as a function of angular location, θ, along the hole circumference. (a) $\mu = 0$, 0.2, and 1, infinite plate, aluminum alloy pin and aluminum alloy plate, (b) $\mu = 0.2$ and 1, infinite plate, and four pin–plate material combinations, (c) $\mu = 0$, infinite plate, and four pin–plate material combinations, (d) $\mu = 0$, finite and infinite plate, and the metallic pin–plate material combinations considered in the study. For metallic pin–plate combinations and small values of friction coefficient, the tangential stress distribution essentially follows a single curve as seen from Fig. 3(b), (e) $\mu = 0.2$ and 1, finite and infinite plate, aluminum alloy pin and aluminum alloy plate and (f) $\mu = 0$ and 0.2, finite plate, two pin–plate material combinations and two types of loading (uniaxial and biaxial).

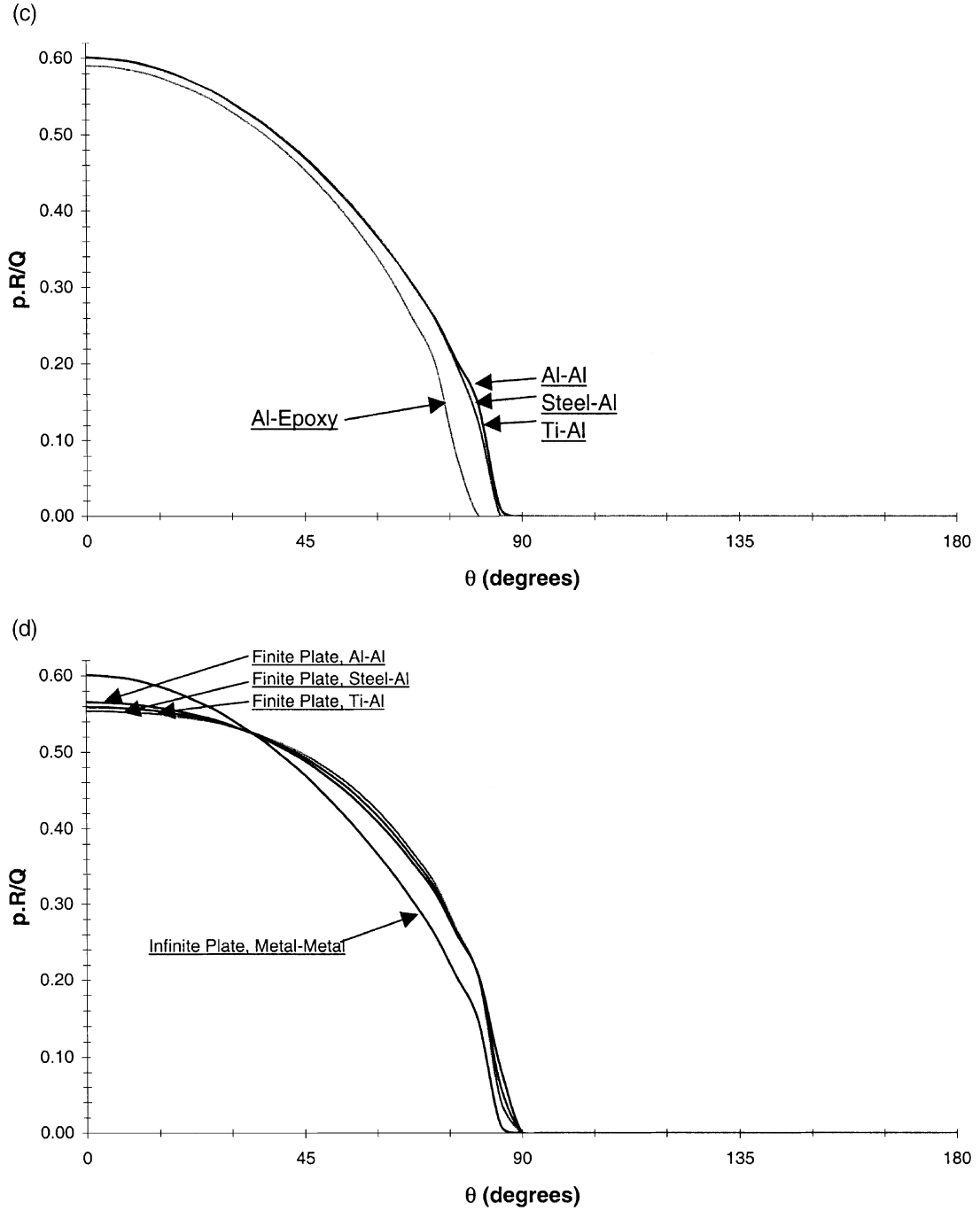

Fig. 3 (*continued*)

contact pressure, $p_0 \cdot R/Q$, decreases significantly with increasing μ. Increasing μ from 0 to 0.2 results in a 16% reduction in $p_0 \cdot R/Q$, while $\mu = 1$ results in an additional reduction of 14%. A slight expansion in the

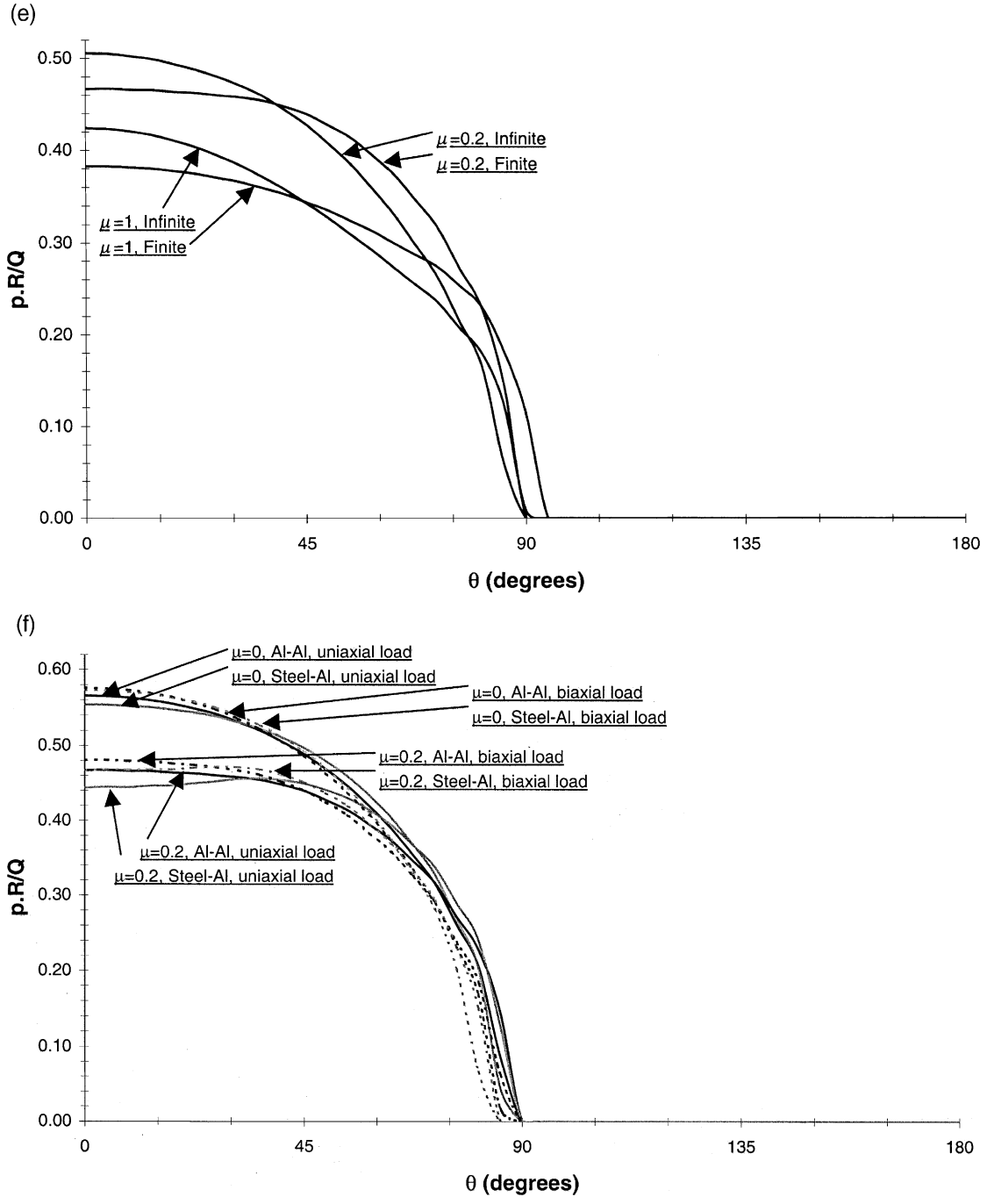

Fig. 3 (*continued*)

contact area, indicated by the contact angle, θ_0, with increasing μ is also noted. In general, the contact pressure distribution tends to "flatten out" as the friction coefficient is increased.

These trends apply equally when the plate dimensions are finite or when the other combinations of pin and plate materials are considered, as seen from Fig. 3(b) and (e). Fig. 3(b) show that the effect of μ on the peak contact pressure increases slightly as the material dissimilarity between the pin and plate increases. The interaction between the friction coefficient and plate dimensions is small.

Effects of material dissimilarity: Fig. 3(c) shows the effect of material dissimilarity on the normalized contact pressure for a connection with an infinite plate and frictionless contact. Apparently, material dissimilarity has no visible effect on the contact pressure distribution when both the pin and plate are metallic (Al, steel or Ti alloy). However, when an aluminum pin is in contact with an epoxy plate, both the peak contact pressure and contact area are noticeably reduced.

Although the effect of material dissimilarity is small when contact is frictionless, it becomes more noticeable as μ increases. Fig. 3(b) shows that the shape of the contact pressure distribution for the aluminum–epoxy combination with $\mu = 0.2$ is altered so dramatically that the peak contact pressure has moved from $\theta = 0°$ to $\theta = +13.5°$ instead. This particular behavior is not seen for the metal–metal pin–plate combinations. The reduction in the peak contact pressure due to material dissimilarity when only the metal–metal combinations are considered, also shown in Fig. 3(b), is less than 2.3% for $\mu = 0.2$ and 10% for $\mu = 1$. Although the effect of material dissimilarity in reducing the peak contact pressure is slightly greater with a finite plate, this is a second-order effect, as seen from Fig. 3(d).

Effects of plate dimensions: Fig. 3(d) also shows the effect of plate dimensions for all-metal alloy connections and frictionless contact. Since the contact pressure is effectively independent of the metal–metal material combination with an infinite plate and frictionless contact (see Fig. 3(c)), the single curve shown for the infinite plate applies to an aluminum, steel or titanium pin. In addition to a change in the shape of the contact pressure distribution, the peak contact pressure is reduced by $(7 \pm 1)\%$ due to the finite plate dimensions regardless of the pin material. The contact area is slightly greater with the finite plate.

Comparison of Fig. 3(d) and (e) shows that the reduction in the peak contact pressure due to the finite plate dimensions can be accentuated very slightly as the friction coefficient increases. The magnitude of the reduction, ~8–9%, is nearly independent of the value of μ for the cases shown. The effect of plate dimensions also increases with the level of material dissimilarity as seen from Fig. 3(d).

Effects of biaxial loading: Fig. 3(f) shows that the peak contact pressure increases slightly under biaxial loading. For the cases considered, this increase is less than 5%. The increase in peak contact pressure is accompanied by a small contraction in the contact area. The figure also shows that the influences of friction coefficient and material dissimilarity are less under biaxial loading than they are under uniaxial loading conditions.

5.2. Tangential stress distribution

The effects of pin–plate friction, material dissimilarity, plate dimensions and biaxial loading on the normalized tangential stress around the hole and stress concentration in the plate systematically follow the effects on the contact pressure described above. For cases involving the finite plate, the applied load is in the form of remote distributed load (stress) and the conventional stress concentration factor (SCF) can be obtained. The SCF, defined as the ratio of the peak tensile stress to the nominal applied stress, is 10 times the peak value of the normalized tangential stress for the finite plate dimensions considered.

Effects of friction: Fig. 4(a) shows the effect of μ on the normalized tangential stress, $\sigma_{\theta\theta} \cdot R/Q$, for an all-aluminum alloy connection with an infinite plate. In general, the bulk stress is tensile everywhere except near $\theta = +180°$, where it becomes compressive. The peak value of $\sigma_{\theta\theta} \cdot R/Q$, and therefore the stress concentration, generally occurs near $\theta = \pm 90°$. This maximum value increases non-linearly from 0.42 to 0.64 as μ increases from 0 to 1. The gradient of the tangential stress near the location of the SCF is also found to increase sharply with μ. Both these changes are accompanied by a reduction in the tensile stresses

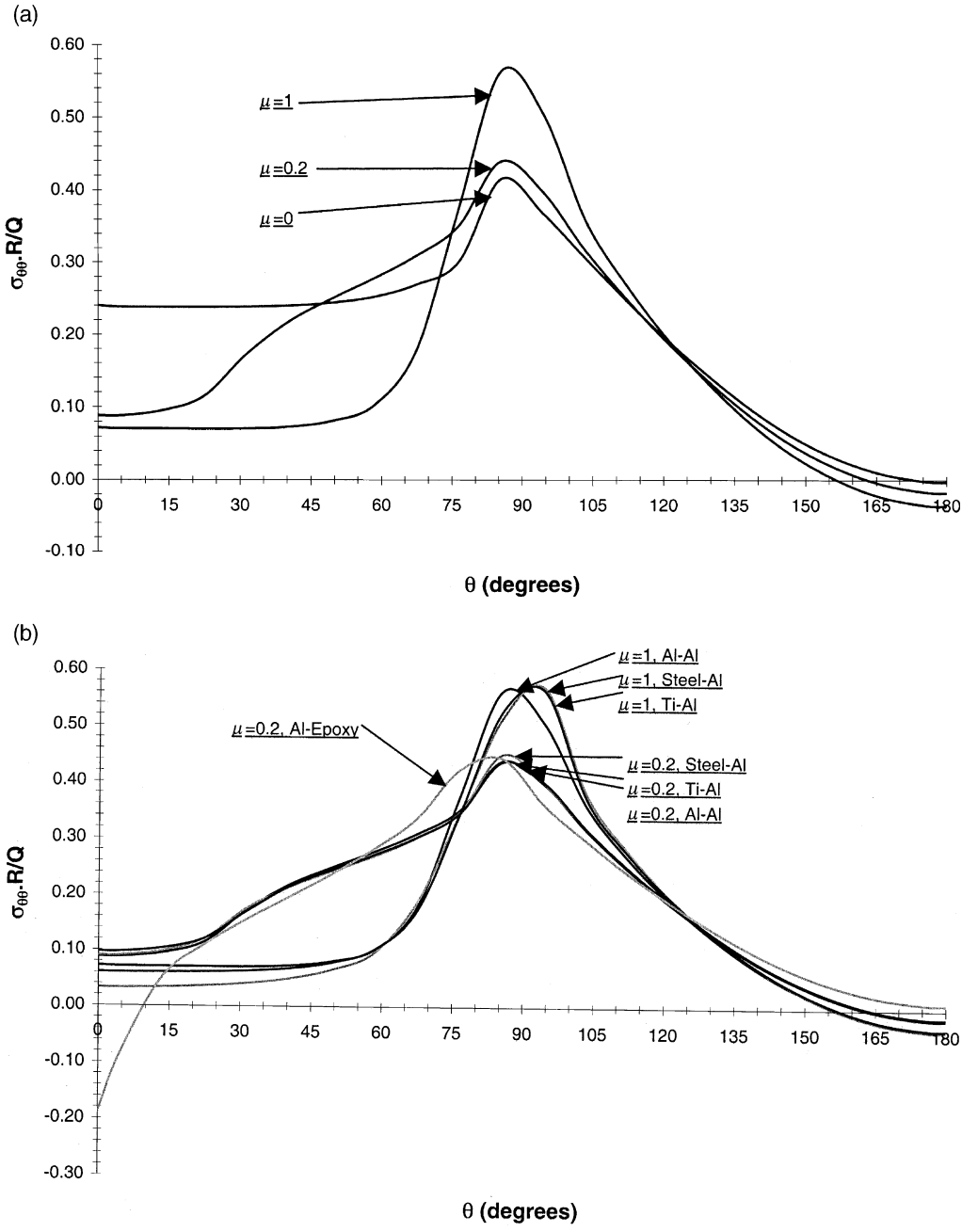

Fig. 4. Normalized tangential stress, $\sigma_{\theta\theta} \cdot R/Q$, around the hole as a function of angular location, θ, along the hole circumference. (a) $\mu = 0$, 0.2, and 1, infinite plate, aluminum alloy pin and aluminum alloy plate, (b) $\mu = 0.2$ and 1, infinite plate, and four pin–plate material combinations, (c) $\mu = 0$, infinite plate, and four pin–plate material combinations, (d) $\mu = 0$, finite and infinite plate, and the metallic pin–plate material combinations considered in the study. For metallic pin–plate combinations and small values of friction coefficient, the contact pressure distribution essentially follows a single curve as seen from Fig. 4(b), (e) $\mu = 0.2$ and 1, finite and infinite plate, aluminum alloy pin and aluminum alloy plate and (f) $\mu = 0$ and 0.2, finite plate, aluminum alloy pin and aluminum alloy plate, and two types of loading (uniaxial and biaxial).

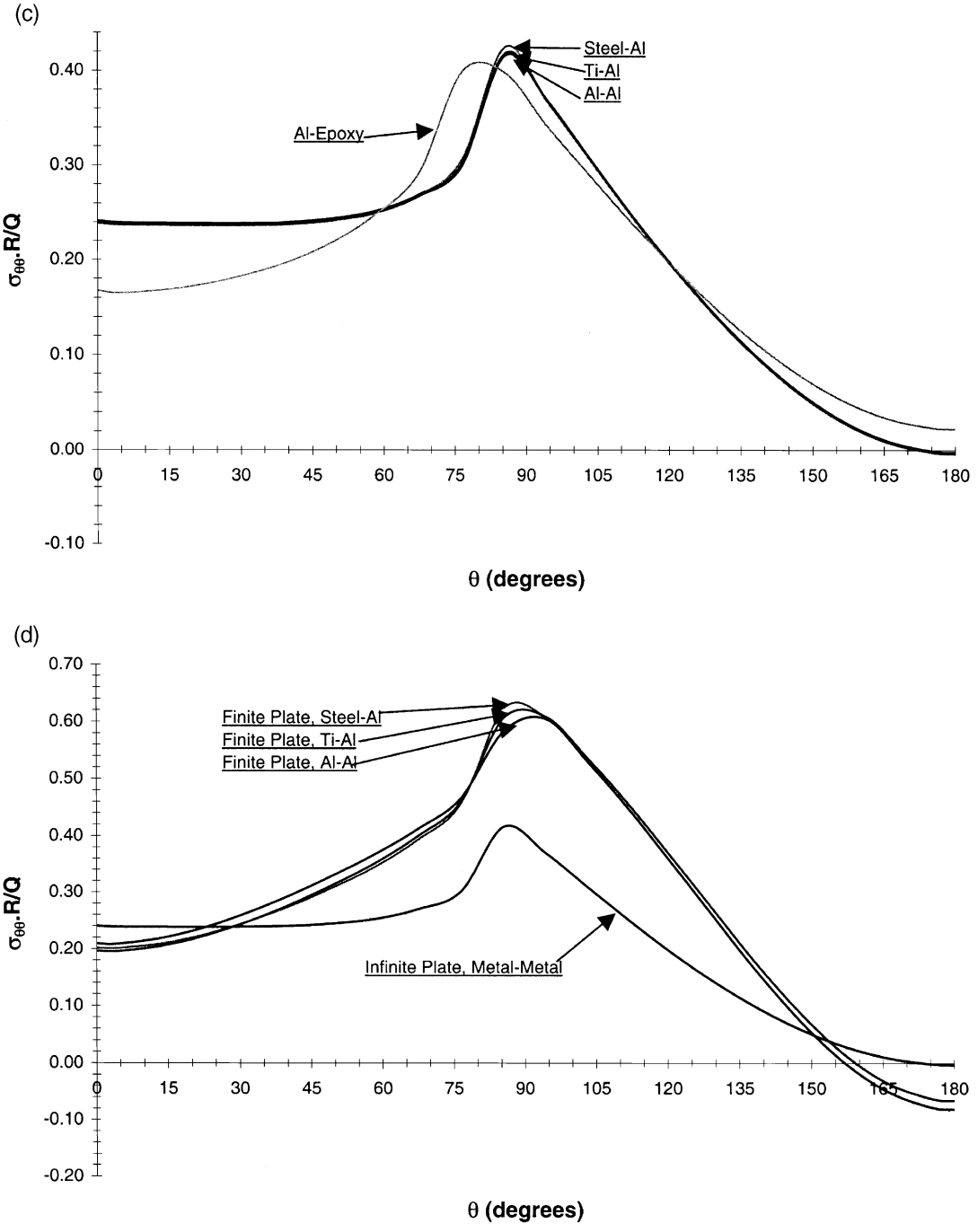

Fig. 4 (*continued*)

over all other angular locations. This reduction is most noticeable over $0° \leqslant \theta \leqslant 90°$, which is the contact region.

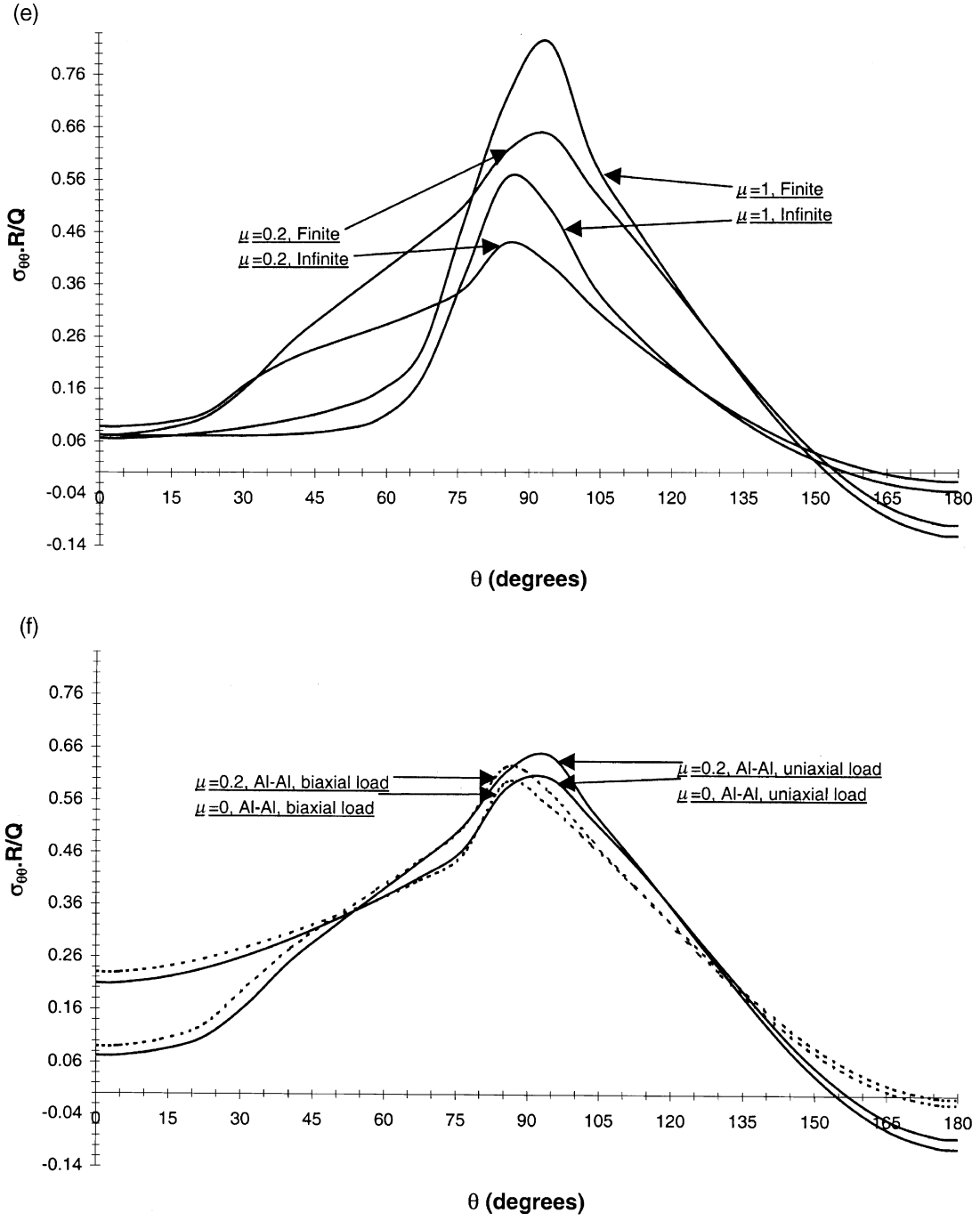

Fig. 4 (*continued*)

The effects cited above are broadly the same regardless of pin material or plate dimensions, as seen from Fig. 4(b) and (e). These figures also show that the effects of friction coefficient on the tangential stress and

SCF are slightly accentuated as material dissimilarity increases and with a finite plate. However, as with the contact pressure, this is a second-order effect.

Effects of material dissimilarity: Fig. 4(b)–(d) show that increasing material dissimilarity leads to a higher SCF with one exception. The SCF with the Al–epoxy combination is 5% less than the SCF with the steel–Al combination for an infinite plate and frictionless contact (Fig. 4(c)). In all the cases considered, the change in the SCF with material dissimilarity is less than 9% regardless of the friction coefficient or plate dimensions.

Effects of plate dimensions: Fig. 4(d) shows that the SCF increases significantly when the finiteness of the plate is considered. The SCF in the finite plate is between 5.9 and 6.2 for the cases shown in Fig. 4(d). With frictionless contact and the metal–metal combinations, the maximum tensile tangential stress with a finite plate is $\sim$1.5 times higher than the value with an infinite plate. Fig. 4(e) shows that the magnitude of this increase is minimally affected by the friction coefficient. As with the contact pressure, the effect of plate dimensions increases with the level of material dissimilarity as seen from Fig. 4(d).

Effects of biaxial loading: Fig. 4(f) illustrates the effect of biaxial loading on the tangential stress distribution and SCF; biaxial loading reduces the SCF. This decrease is found to be 3.4% and 7.1% for $\mu = 0$ and 0.2, respectively, and the aluminum–aluminum pin–plate material combination.

6. Discussion

The stress concentration factors reported here are in reasonable agreement with the well-known, experimentally measured values due to Frocht and Hill (1940). For example, they report an SCF of 6.9 [1] for an all-aluminum connection with the same relative dimensions considered in this study (plate width to hole diameter ratio of 0.2 (=2(3.06)/30.6) and head distance [2] to plate width ratio of 0.5 (=15.3/30.6); the friction coefficient in their experiments is not known). In comparison, the SCF from the present analyses is 6.5 when $\mu = 0.2$ and 8.2 when $\mu = 1$ (see Fig. 4(e)).

The results show that the friction coefficient, material dissimilarity and plate dimensions interact in a complicated manner to modify each other's effects on the contact pressure and tangential stress distributions. The effect of the friction coefficient on the contact pressure and tangential stress distributions is significant even with identical materials and finite or infinite plate dimensions. In comparison, the effect of material dissimilarity is very small for frictionless contact and only increases as the friction coefficient increases or if the plate is finite. In either case, the magnitude of this increase is relatively small. Based on these considerations, pin–plate friction is a more important design variable than the material combination in realistic connections, which necessarily consist of finite plates.

Since a higher friction coefficient at the pin–plate interface reduces the peak and average values of the contact pressure distribution, and increases the SCF and its gradient, minimizing friction would be most beneficial to the strength of the connection. This should also improve the fretting resistance since increasing contact pressure has a beneficial effect on fretting fatigue life (Iyer, 2001).

The increase in the maximum tensile tangential stress around the hole when the plate has finite dimensions is also significant from a design standpoint. Plate finiteness changes the peak contact pressure and SCF significantly but this is nearly independent of the friction coefficient in the cases considered here. Therefore, as a first approximation, it can be regarded as an independent design variable. The study shows

[1] Frocht and Hill (1940) define SCF values based on the nominal net section stress instead of the gross stress. The value of 6.9 is obtained by considering the gross stress.

[2] The head distance is measured from the center of the pin to the free (unloaded) end of the plate along its longitudinal axis.

that a safety factor of 2 used in conjunction with the solution for an infinite plate would, in fact, provide a much smaller margin of safety. Referring to Fig. 4(e) and (f), the SCF is greater by ~50% when the plate is finite and biaxially loaded (aluminum pin and plate and $\mu = 0.2$). This translates to a difference of ~360 MPa under a remote, nominal stress of 120 MPa, which is a common occurrence in practice. The contact width is found to be between 6% and 11% smaller when the plate is infinite for the cases considered. The diminished load bearing area provides a rationale for the elevated contact pressures observed with an infinite plate.

The finding that material dissimilarity has a small effect on the contact pressure and tangential stress distribution in many common scenarios, i.e. a metallic pin in frictional contact with a finite metallic plate, confirms a similar finding by Frocht and Hill (1940). This means that it is advantageous to use titanium or aluminum instead of steel to rivet aluminum plates for increasing structural strength while reducing weight at the same time. The four material pairs considered in the present study reflect traditional and more recent material combinations used in aerospace and automotive structures.

The results presented are valid for elastic, two-dimensional pinned connections and three-dimensional butt (double shear) joints. However, in single shear riveted or bolted connections, three-dimensional aspects such as plate bending, rivet tilt, plate–plate contact and countersinking cannot be neglected and the stress concentration factor for the plate can be as high as 12 (Iyer et al., 1999). For these cases, the present analyses offer lower-bound estimates of the SCF because the pin has not been allowed to tilt or shear. Additional factors such as pin–hole radial interference, load-level effects, plasticity and head distance are also important and warrant separate consideration. The finite element model can, however, be modified to account for these factors.

7. Conclusions

The contact area, contact pressure and tangential stress distributions in a pinned connection can be modified significantly and in a complex manner by the pin–plate friction coefficient, material combination and plate dimensions. It is shown that consideration of plate finiteness can increase the stress concentration in the plate by ~50%. Between the two remaining factors, the friction coefficient is primary – increasing friction reduces the peak contact pressure and increases the stress concentration in the plate by significant amounts. The magnitude of the friction coefficient also directly determines the magnitude of the effect of pin–plate material dissimilarity. In all cases, existing closed-form solutions for the stress concentration in the plate are non-conservative when compared with the solutions for realistic contact conditions. These findings can be used to enhance the design of double shear bolted and riveted connections.

Acknowledgements

The initial portion of this study was supported by grants from the Air Force Office of Scientific Research (F49620-93-1-0488 and F49620-93-1-0268). The author wishes to thank G.T. Hahn, C.A. Rubin and J.R. Barber for their useful comments. P. Decuzzi assisted with the plots in Fig. 2.

References

Barber, J.R., 1992. Elasticity. Kluwer, The Netherlands.

Ciavarella, M., Decuzzi, P., 2000. The state of stress induced by the plane frictionless cylindrical contact in the case of elastic similarity. Int. J. Solids Struct., submitted for publication.

Crawley, E.F., Sarver, G.L., Mohr, D.G., 1983. Experimental measurement of passive material and structural damping for flexible space structures. Acta Astronautica 10 (5–6), 381–393.

Folkman, S.L., Roswell, E.A., Ferney, G.D., 1995. Influence of pinned joints on damping and dynamic behavior of a truss. J. Guid. Ctrl. Dyn. 18 (6), 1398–1403.

Frocht, M.M., Hill, H.N., 1940. Stress-concentration factors around a central circular hole in a plate loaded through pin in the hole. J. Appl. Mech. 7, A5–A9.

Gaul, L., Lenz, J., Sachau, D., 1998. Active damping of space structures by contact pressure control in joints. Mech. Struct. Mach. 26 (1), 81–100.

Ho, K.C., Chau, K.T., 1997. An infinite plane loaded by a rivet of a different material. Int. J. Solids Struct. 34 (19), 2477–2496.

Iyer, K., Rubin, C.A., Hahn, G.T., 1999. Three-dimensional analyses of single rivet-row lap joints – Part I: elastic response. Recent Advances in Solids and Structures, PVP – Vol. 398. ASME, New York, pp. 23–40.

Iyer, K., 2001. Peak contact pressure, cyclic stress amplitudes, contact semi-width and slip amplitude: Relative effects on fretting fatigue life. Int. J. Fatigue 23 (3), 193–206.

Johnson, K.L., 1985. Contact Mechanics. Cambridge University Press, Cambridge.

Lin, S., Hills, D.A., Nowell, D., 1997. Stresses in a flat plate due to a loose pin pressing against a cracked hole. J. Strain Anal. Engng. Des. 32 (2), 145–156.

Schijve, J., 1996. Fatigue Crack Growth Under Variable-Amplitude Loading. ASM Fatigue and Fracture Handbook, vol. 19, ISBN 0-87170-385-8.

Shin, Y.S., Iverson, J.C., Kim, K.S., 1991. Experimental studies on damping characteristics of bolted joints for plates and shells. ASME J. Pressure Vessel Technol. 113 (3), 402–408.

Timoshenko, S.P., Goodier, J.N., 1961. Theory of Elasticity. McGraw-Hill Book Company, New York.